Application of scanning probe energy loss spectroscopy to SERS-active metal nanostructures

Journal of Physics: Conference Series **1866** (2021) 012006 doi:10.1088/1742-6596/1866/1/012006

Application of scanning probe energy loss spectroscopy to SERS-active metal nanostructures

M Beshr[1], G Amarandei[2], A D Meade[3], R E Palmer[4] and S Murphy[1]

[1] Centre of Applied Science for Health (CASH), Technological University Dublin, Tallaght Campus, D24 FKT9, Ireland
[2] School of Physics & Clinical & Optometric Sciences, Technological University Dublin, City Campus, Kevin Street, D08 NF82, Ireland
[3] Centre for Radiation and Environmental Science, FOCAS Research Institute, Technological University Dublin, City Campus, Kevin Street, D08 NF82, Ireland
[4] College of Engineering, Swansea University, Swansea, SA1 8EN, United Kingdom

E-mail: shane.murphy@tudublin.ie

Abstract. Surface-enhanced Raman spectroscopy (SERS) relies on adsorbing target molecules onto metal nanostructures where the light can resonantly couple with localised surface plasmon resonances. These plasmons can be tuned by changing the nanostructure size, shape, spacing and composition, but this is a complex process. Therefore, having an experimental method that can directly map the plasmons would be extremely useful for developing SERS-active substrates. This paper investigates the possibility of applying a novel scanning probe method, scanning probe energy loss spectroscopy, to map the plasmonic behaviour of SERS-active metal nanostructures in order to optimise their enhancement factor and reproducibility.

1. Introduction

Raman spectroscopy uses the inelastic scattering of light to probe the characteristic vibrational modes of target molecules in an analyte and thus provide unambiguous chemical identification. Conventional Raman spectroscopy is limited by a low signal intensity, as only about one in 10^6-10^8 photons is inelastically scattered. In surface-enhanced Raman spectroscopy (SERS), the signal is enhanced by adsorbing the target molecule onto a nanostructured metal substrate, where light can resonantly couple with localised surface plasmon resonances (LSPR). This leads to a local electric field enhancement near the nanostructure surface that can boost the Raman signal by a factor of 10^6-10^8 [1]. The enhancement is maximised when the LSPR frequency lies between that of the incident and Raman-scattered photons, and may be tuned by tailoring the nanostructure size, shape, spacing and composition. The design of these nanostructured surfaces is often based on simulations of the plasmonic behaviour of ideal nanostructures using methods such as the finite-difference time-domain (FDTD) method [2] and discrete dipole approximation (DDA) [3]. However, the behaviour of real-world samples can be more complex due to inhomogeneities or defects arising from the fabrication process. Having an experimental technique that is capable of directly imaging the LSPR behaviour of nanostructure ensembles would be extremely useful for advancing the development of SERS-active substrates. Plasmon mapping of individual metal nanostructures has previously been demonstrated using scanning near-field optical microscopy (SNOM) [4], cathodoluminescence (CL) spectroscopy [5] and

scanning transmission electron microscopy with electron energy loss spectroscopy (STEM-EELS) [6]. In this paper, we propose an alternative method, scannning probe energy loss spectroscopy (SPELS) [7], which may be applied to investigate the plasmonic behaviour of SERS-active metal nanostructures. SPELS is a variant of scanning tunneling microscopy (STM) in which the tip is biased in the field-emission regime rather than the tunneling regime. Electrons are field-emitted from the tip and are collected by an energy analyser after interaction with the sample surface.

2. Experiment

The experimental configuration of the SPELS instrument has been described elsewhere [8, 9]. Briefly, an electron energy analyser is positioned in close proximity to the sample surface in an ultrahigh vacuum STM. The STM is modified by adding grounded shielding around the piezo scanner assembly and replacing the in-vacuum op-amp with an external amplifier that can be by-passed for field-emission measurements. The analyser is set at an angle of 7° with respect to the surface plane as the reflected electron signal is maximised near the surface plane due to the deflection of these electrons by the electric field between the tip and sample [10]. The tip can be negatively biased at a voltage up to 400 V with respect to the sample to stimulate the field-emission of electrons from the tip. The field-emission current is measured at the sample with a Keithley 6485 picoammeter to produce constant field-emission current images of the surface [8]. The energy of electrons reflected from the sample surface is measured by the energy analyser to produce an energy loss spectrum, where electronic phenomena in the sample, such as plasmon resonances and interband transitions, are recorded as energy loss peaks. Spectroscopic data are acquired simultaneously with the topographic data provided by the field-emission images.

3. Results

A sequence of constant field-emission current images measured of Ag islands grown at 610 °C on graphite is shown in Fig. 1. An STM image of the same area, taken directly after the field-emission measurements, is shown for comparison. All images were taken with the same current setpoint of 100 pA, but with the tip bias varied between 60 mV and 80 V. It can be seen that the images taken at low field-emission bias compare well with the STM image. The loss of surface resolution occurs gradually in the voltage range from 20 V to 75 V, after which there is a rapid loss of resolution, with only the largest feature still visible at a field emission bias of 80 V. Constant field-emission current imaging may be particularly useful when measuring surface features with high aspect ratios, where the close tip-sample separations required by STM can lead to large tip convolution effects. Field-emission measurements benefit from larger tip-sample separations and are capable of providing accurate measurements of surface dimensions at low field-emission bias. However, the imaging characteristics are specific to the field-emission characteristics of each tip used, and are susceptible to large, irreversible changes during measurement, particularly at higher bias values.

The effect on the sample due to the field produced by the tip can be seen in Fig. 2, which shows a sequence of 100 nm × 100 nm STM and field-emission images measured on the same area of an Au(111) surface. The spatial resolution of the field-emission imaging is demonstrated by the fact that it is possible to resolve the monatomic steps on the Au(111) surface using a tip bias of 15 V. However, field-emission imaging also results in the roughening of the surface, which becomes more pronounced when the tip bias is increased to 20 V. The tip-sample separation during the field-emission imaging is 2-5 nm in Figs. 2(b) and (d). The surface roughening is caused by the ejection of Au atoms from terrace sites at the base of the monatomic steps and agglomerate into three-dimensional nanoparticles on the Au terraces.

Figure 3 shows a set of simultaneously-acquired SPELS data measured on a Ag island on graphite using a 30 × 30 measurement grid, a field-emission current of 2 μA and a tip bias of 110 V. Figure 3(a) shows the constant field-emission current image of the topography of the

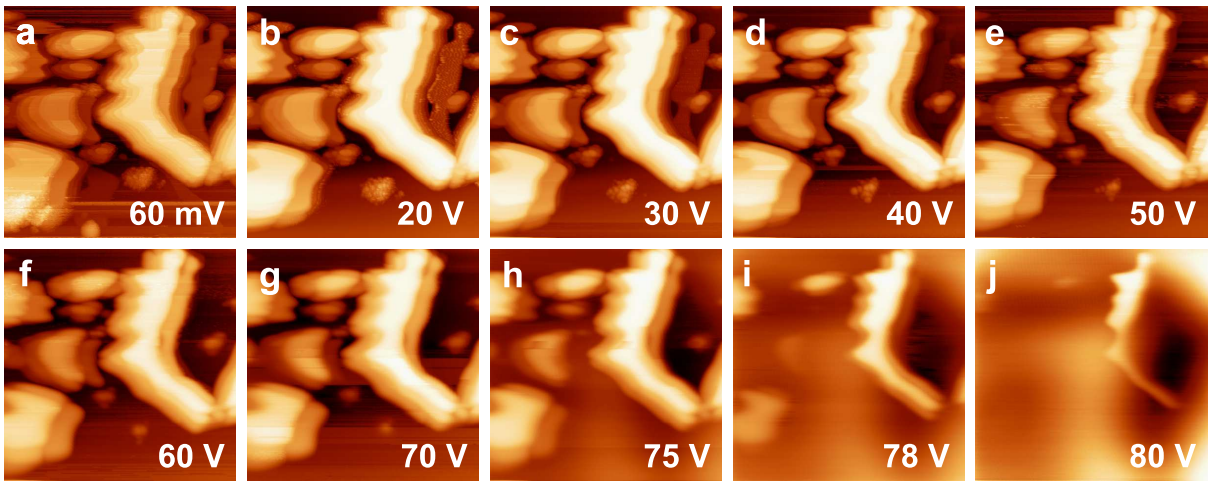

Figure 1. 2 μm $\times$ 2 μm images of Ag islands on graphite measured with the STM operating in the tunneling and field-emission regimes. The STM image (a) was obtained using I = 100 pA and U = 60 mV, while the field-emission images (b-j) were taken with I = 100 pA and U = 20-80 V.

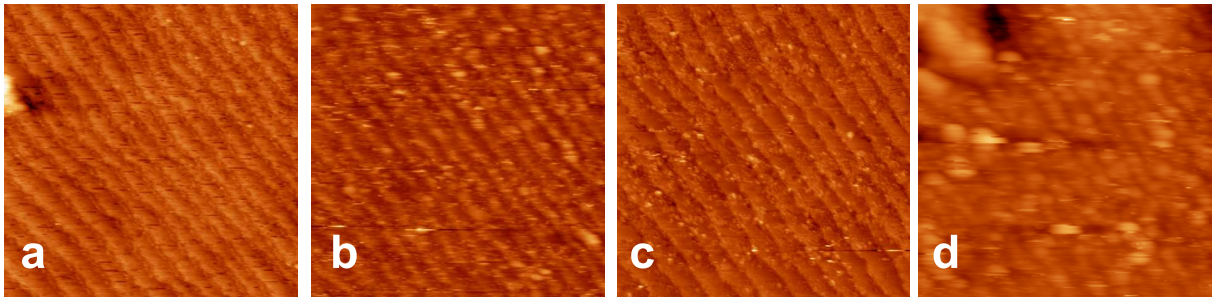

Figure 2. Series of 100 nm $\times$ 100 nm images taken in sequence of the same area of an Au(111) surface. (a) and (c) STM images measured with I = 600 pA and U = 100 mV. (b) and (d) Field-emission images taken with I =600 pA and (a) U = 15 V and (b) U = 20 V.

Ag island, while Fig. 3(b) shows the reflected electron current collected by the electron energy analyser. It is consistently observed that the Ag islands yield a lower average reflected electron current than the surrounding graphite substrate. The reason for this is not clear, though contrast reversal is observed in the case of low-energy scanning electron microscopy [11]. However, it is worth noting that the spatial resolution of the reflected electron image is better compared to that of the field-emission current image. Figure 3(c) shows the energy loss spectrum obtained by summing the EELS spectrum collected at each point in the measurement grid. The loss peak associated with the Ag plasmon is visible at 3.6 eV. Normalising the area under this peak to the area under the zero-loss peak at each point in the measurement grid is used to obtain the image in Fig. 3(d), which maps the silver plasmon intensity across the image.

While Fig. 3(d) only maps a single plasmon loss feature, it has previously been demonstrated that smaller structures such as Ag nanoprisms and Au nanorods display distinct plasmon loss features that may be separated in energy by 0.5 eV or more. For example, in the case of Ag nanoprisms with a side length of 78 nm and thickness of 10 nm, Nelayah et al. [6] observed plasmon loss peaks at 1.75, 2.70 and 3.20 eV using STEM-EELS, corresponding to measurement of different modes at the corner, edge and centre of the nanoprism, respectively. N'Gom et al. [12] measured plasmon loss peaks at 1.9 and 2.4 eV corresponding to longitudinal and transverse

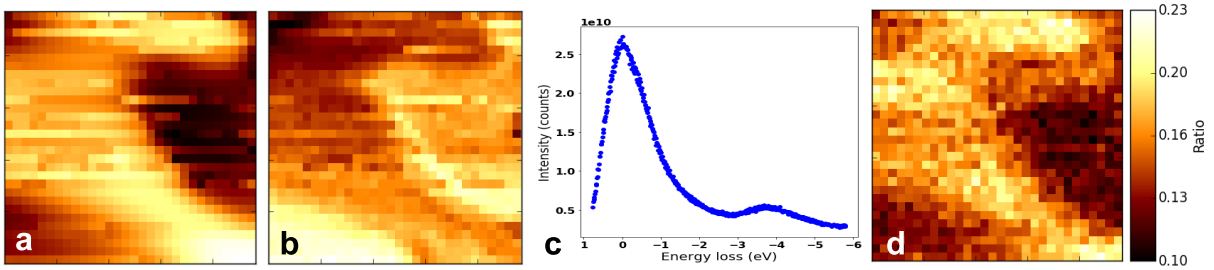

Figure 3. (a) 2 μm $\times$ 2 μm constant field-emission current image of Ag island on graphite measured over a 30 $\times$ 30 grid with I = 2 μA and U = 110 V. (b) Total electron count measured simultaneously by the electron energy analyser. (c) Electron energy loss spectrum showing Ag plasmon loss peak at 3.6 eV. (d) Plasmon loss map obtained by normalising the area under the plasmon loss peak by the area under the zero-loss peak at each point in measurement grid.

modes in Au nanorods 70 nm long and 28 nm wide. Further peaks shifts were observed due to the dipolar coupling between closely-spaced neighbouring nanorods. As the spectral resolution of SPELS is estimated to be 1 eV [7], it suggests that it may also be possible to map some of these different plasmon modes using SPELS.

4. Conclusion

Modifying a UHV STM to perform field-emission and SPELS measurements can greatly extend its capabilities. Field-emission imaging at low tip bias can provide accurate measurements of surface topography and may be particularly useful for imaging high-aspect ratio structures. SPELS measurements can reveal spectroscopic features that can be used to unambiguously identify sample composition. The results presented here suggest that SPELS may be a useful tool for mapping the plasmon response of metal nanostructures such as those encountered in SERS-active substrates as plasmon loss features can be mapped with a spectral resolution of 1 eV and a spatial resolution of around 50 nm. Future work will focus on mapping the plasmon modes in well-defined geometric nanostructures such as Ag nanoprisms, on developing better control and reproducibility of the field-emission characteristics of the tip, and characterising sample stability in the presence of large electric fields.

5. Acknowledgments

SM acknowledges support from the University of Birmingham, UK through the provision of equipment. MB acknowledges support from the Irish Research Council through a Government of Ireland postgraduate scholarship (GOIPG/2020/1572).

6. References

[1] Li W, Zhao X, Yi Z, Glushenkov A M and Kong L 2017 *Anal. Chim. Acta* **984** 19
[2] Yao G Y, Liu Q L and Zhao Z Y 2018 *Catalysts* **8** 236
[3] Amendola V 2016 *Phys. Chem. Chem. Phys.* **18** 2230
[4] Rang M, Jones A C, Zhou F, Li Z Y, Wiley B J, Xia Y and Raschke M B 2008 *Nano Lett.* **8** 3357
[5] Edwards P R, Sleith D, Wark A W and Martin R W 2011 *J. Phys. Chem. C* **115** 14031
[6] Nelayah J et al. 2007 *Nature Phys.* **3** 348
[7] Palmer R E, Eves B J, Festy F and Svensson K 2002 *Surf. Sci.* **502-503** 224
[8] Murphy S, Bauer K, Sloan P A, Lawton J J, Tang L and Palmer R E 2015 *Appl. Phys. Express* **8** 126601
[9] Bauer K, Murphy S and Palmer R E 2017 *Nanotechnology* **28** 105711
[10] Eves B J, Festy F, Svensson K and Palmer R E 2000 *Appl. Phys. Lett.* **77** 4223
[11] Müllerová I and Frank L 2004 *Scanning* **26** 18
[12] N'Gom M, Li S, Schatz G, Erni R, Agarwal A, Kotov N and Norris T B 2009 *Phys. Rev. B* **80** 113411